A Unified Design of ACO and Skewness based Brain Tumor Segmentation and Classification from MRI Scans

Umaira Nazar Hussain[1], Muhammad Attique Khan[2], Ikram Ullah Lali[3]

[1] Department of CS & IT, University of Sargodha, Pakistan

[2] Department of CS & E, HITEC University, Museum Road, Taxila, Pakistan

[3] Department of CS, University of Gujrat, Pakistan

Corresponding Author*: *attique@ciitwah.edu.pk*

Abstract: Brain tumor is among the major reasons of deaths among cancerous diseases around the world. Medical imaging technologies use to detect brain tumor is very popular these days. However, before time detection is an open ended research and needs more accuracy. Multimodality medical image fusion has emerged with promising results in cancer detection. In this paper, a hybrid technique for extracting tumor using MRI images is presented. This technique consists of five steps such as de-noising of image, extraction of tumor, feature selection, feature fusion and classification. Curvelet transformation is implemented in the first step for image de-noising. Then in the second step, Ant Colony Optimization (ACO) is utilized along Thresholding method for extraction of tumor based on MRI scans of brain. Three distinct kinds of features are extracted depends on texture and shape in the third step. After that, top 70% features are selected based on priority approach and fusion is performed using concatenation based approach. In the last step, fused features are fed to different classifiers such as SVM. The proposed technique is tested on two datasets named as BRATS 2013 and private dataset. The proposed system performance is well as compared to different present techniques.

Keywords*:* Brain Tumor; Tumor segmentation; Feature extraction; Features Reduction; Classification

1. INTRODUCTION

A brain tumor is a collection of unusual or abnormal cells present inside a brain. The rigid outer covering of brain which plays a role of protector for it in case of an injury is its skull. Any abnormal growth of cells inside it will cause a severe problem. The brain tumor is of two types- malignant which is more dangerous and difficult to cure while the second type is benign which is curable if detected at initial stage (Sharif, Tanvir, Munir, Khan, & Yasmin, 2018). Moreover, the two categories of brain tumor are known as primary and metastatic. The primary brain tumor starts within the brain due to the abnormal growth of brain cells but in contrast, metastatic starts when cancer cells from other parts of body are fragmented and travel towards the brain. Due to this reason, metastatic brain tumors always lie in the category of malignant but primary brain tumor cannot be malignant all time, it may lie in benign too (Liu et al., 2014). Treatment of brain tumor varies according to its categories. In United States, currently around 700,000 people are diagnosed with primary brain cancer and more than 790,000 will be identified in 2018 (Buerki, Chheda, & Okada, 2018). The brain tumor has a great psychological, cognitive and physical impact on the quality of patient's life as well as it totally alters everything for patients and their relatives.

Brain tumors are classified according to tumor location, tissues involved and the type of tumor that is benign or malignant. The selection of treatment therapy for a brain tumor depends upon the size, location and its growth rate (Anitha & Siva Sundhara Raja, 2018). World Health Organization (WHO) gave the grading scheme of brain tumors. According to this scheme, tumors are categorized in four grades under a microscope and these grades are given name as I, II, III, and IV grade respectively. Furthermore, benign tumor known as low-grade brain tumor because it consists both I grade as well as II grade tumors. While on the other side malignant tumor known as high-grade brain tumor because it has tumors of III grade and IV grade. The rate to detect low-grade brain tumor at starting stage or initial stage is very low and hence it gets converted to high-grade brain tumor (Roberts et al., 2018). The brain image of malignant tumor, healthy brain, and benign tumor are shown in Figure 1. Magnetic resonance image (MRI) as well as Computed Tomography (CT) are two frequently used modalities of imaging which play a vibrant role for detecting tumor in the brain(Drozdzal et al., 2018). MRI scan of brain and CT both help doctors to identify and detect the exact location and size of a tumor in brain. MRI is a modality with a better contrast of soft tissues and it is non-invasive which gives details about tumor location, shape and size in the absence of high ionization radiations (Mohsen, El-Dahshan, El-Horbaty, & Salem, 2018).

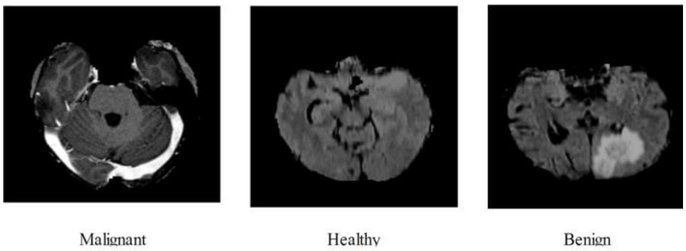

Figure 1: Sample brain tumor MRI images

MRI images have some benefits as compared to other modality images because these images help doctors to detect tumor at an initial stage by giving a clear image with more details (Kalavathi & Prasath, 2016). The MRI images are classified into four modalities which are known as T1 modality, T1c modality, T2 modality and T2f modality respectively. Further, these modalities play a prominent part in the detection of tumor area in brain image. The sample scans are shown in Figure 2.

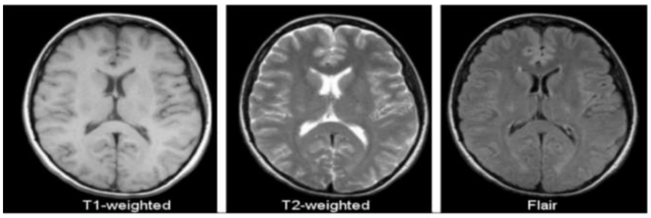

Figure 2: Sample scans of brain modalities *(Zhang et al., 2015)*

Manual detection and segmentation of brain tumor do not provide accurate results and it is time taking and slow process. The main limitation of manual method is its irreducibility which increases demand for computer-based segmentation and classification. Moreover, tumor shape, tumor diameter, texture, size, location and irregularity are common problems in existing systems. To overcome these problems, in this research, an amalgamation approach is utilized which includes series of primary steps- curvelet transform based tumor visibility enhancement, ACO and thresholding based tumor segmentation, texture and shape feature extraction, priority features selection and finally classification. Major contributions are:

- Curvelet transform is employed to enhance the visibility of original tumor from a distinct scale and angle.
- The tumor segmentation is performed through ACO along with thresholding approach.
- Multi-type features are extracted like shape and texture. Then a new approach is applied named as PCA reduced Skewness (PCArS) approach for irrelevant features reduction.
- A comparison is conducted with several classification methods and existing techniques for the validity of this approach.

1.1. Problem Statement

The work presented in this article, deals with the several challenges including: a) low contrast video acquisition because of complex background; b) variations in the human viewpoint; c) occlusion between human and other objects; d) measurement of the body size, symmetry and support level of a human at the time of performing the action because each person has different body size and style; e) high dimensions of extracted features, and f) selection of most useful features. These listed challenges degrade the performance of HAR. In addition, the high dimensional features increase the computational time of automated framework.

2. RELATED WORK

Automatic identification and classification of harmful human diseases such as brain tumor, stomach infections, skin cancer and lungs cancer are very common infections in medical imaging. There exists several segmentation and classification methods based on machine learning (ML) and computer vision (CV) which are utilized for the diagnosis of these infections (Akram, Khan, Sharif, & Yasmin, 2018; Khan, Akram, Sharif, Awais, et al., 2018; LIAQAT et al., 2018; Nasir et al., 2018; Sharif et al., 2017). The brain tumor is a critical and most dangerous type of cancer in medical imaging and recently various computerized methods are introduced for its diagnosis. In general, existing methods consist of many steps such as preprocessing for noise removal, segmentation of tumor area, useful features extraction, reduction of redundant features, and classification (Sharif, Tanvir, et al., 2018). Ariyo et al. (Ariyo, Zhi-guang, & Tian, 2017) introduced a technique named as SFCMKA (Spatial Fuzzy C-Means and K-means Algorithm) for the separation of abnormal brain tissues from the healthy brain tissues. In this technique, the noise is mitigated due to the merging of spatial function to FCM algorithm and maximum probability for pixels with singular membership is attained by using K-means algorithm. Sharif et al. (Sharif, Tanvir, et al., 2018) described an improved binomial thresholding and multi-features selection approach for brain tumor segmentation. Gaussian filter is used for pre-processing and improved thresholding technique with some morphological operations is utilized for tumor segmentation. After that, a serial based method is implemented for the fusion of extracted geometric and Harlick features. Lastly, selection of best features is performed from the fused vector using GA and classification is performed using LSVM on the basis of these best features. Damodharan et al.(Damodharan & Raghavan, 2015)introduced a brain tumor detection approach which depends on the integration of Tissue Segmentation and Neural Network. The performance of implemented approach is measured by comparing its results with other classification approaches such as NN, KNN and Bayesian classification with respect to accuracy, specificity and sensitivity. Pereira et al. (Pereira, Pinto, Alves, & Silva, 2016)implemented an approach based on Convolution Neural Networks (CNN) using MRI images for the accurate extraction of tumor. Rajuet al. (Bahadure, Ray, & Thethi, 2018)implemented a classification method based on Bayesian fuzzy clustering for extraction and classification of tumor from MRI scans. The presented method performance is good in terms of accuracy as compared to few already implemented approaches. Sharma et al. (Sharma, Purohit, & Mukherjee, 2018)introduced a hybrid approach extraction of tumor region accurately as well as classification of brain tumor. Three primary steps are involved in this presented approach- (a) Preprocessing which included thresholding, morphological operations and watershed segmentation (b) Segmented MRI scans are used for extraction of GLCM features, and (c) classification of tumor through KMNN classifier.

3. PROPOSED METHOD

There are five steps of proposed system including pre-processing of an input image, segmentation of tumor using ACO and thresholding, extraction of few useful features, best features selection based on high priority and fusion of features. Later on these features are given for classification process to a classifier named as Support Vector Machine (SVM). The demonstration of flow of proposed approach is presented in **Figure 3**.

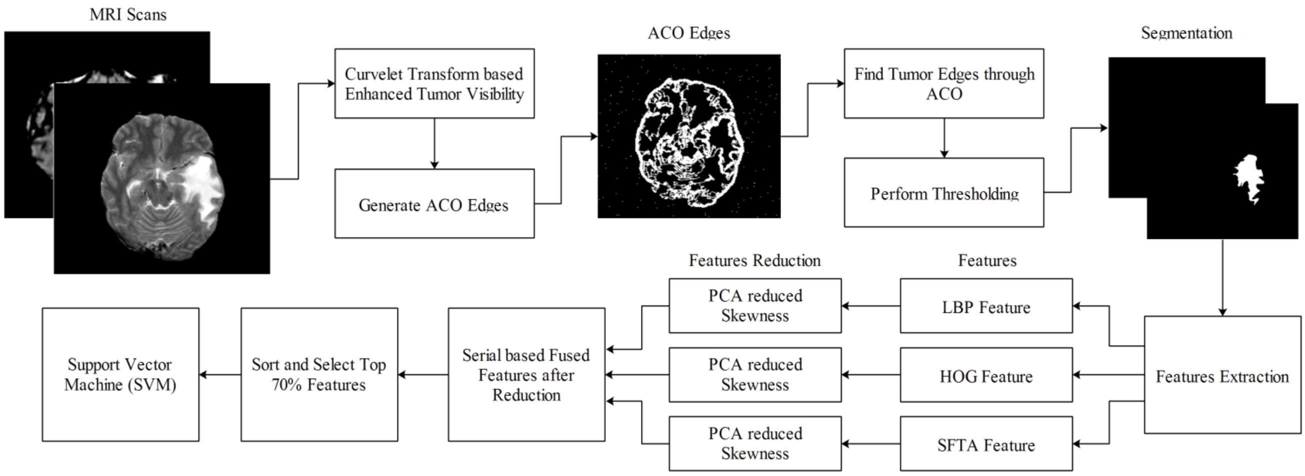

Figure 3: Proposed brain tumor extraction and classification approach using MRI scans

3.1. Image Enhancement Using Curvelet Transform

Curvelet transform is implemented for mitigation of the unwanted noise from an input image of brain by enhancing the tumor region. This enhancement technique is good in terms of implementation simplicity, disorder stability and less processing time. Furthermore, maximum recovery of edges and faint linear and curve features are attained in Curvelet transform. The use of ridgelet transforms make Curvelet transform(Routray, Ray, & Mishra, 2018; Starck, Candès, & Donoho, 2002) efficient as compared to wavelet transform in terms of best performance for image de-noising. The ridgelet transform is converted to Radon transform. Anisotropy scaling relationship is performed to implement support interval or scaling in ridgelet transform. The curve or edge is decomposed into blocks and sub-blocks by applying multi-scaling ridgelet. Further, these sub-blocks are roughly considered as straight lines for implementation of ridgelet analysis. The decomposition stages of Curvelet transform are mathematically described as follows in equation (1).

$$\mathrm{g} \mapsto (\mathrm{F_0\, g}, \Delta_1 \mathrm{g}, \Delta_2 \mathrm{g}, \ldots\ldots) \qquad (1)$$

Where, $\mathrm{F_0}$ denotes sub-bands filters,Δdenotesinformation about sub-band 2^{-2b} and g is an object like tumor.

The smooth windows are $\mathrm{V_Q}(\mathrm{x}_{1,}\mathrm{x}_2)$ and diadic squares are used to localize these smoothing windows. The mathematical relation is explained below in equation (2).

$$\mathrm{Q} = \left[\frac{\mathrm{K}_1}{2^{\mathrm{b}}}, \frac{(\mathrm{K}_1+1)}{2^{\mathrm{b}}}\right] \times \left[\frac{\mathrm{K}_2}{2^{\mathrm{b}}}, \frac{(\mathrm{K}_2+1)}{2^{\mathrm{b}}}\right] \qquad (2)$$

After that, renormalization is performed on resultant square to unit scale. The quantitative relation of this step is represented mathematically as follows.

$$\mathrm{h_Q} = \mathrm{F^{-1}}_{\mathrm{Q}}\left(\mathrm{V_Q} \Delta_{\mathrm{b}} \mathrm{g}\right), \mathrm{Q} \in \mathrm{Q_b}$$

Where, $(\mathrm{F_Q g})(\mathrm{x}_{1,}\mathrm{x}_2) = 2^{\mathrm{b}}\, \mathrm{g}(2^{\mathrm{b}}\, \mathrm{x}_1 - \mathrm{K}_1, 2^{\mathrm{b}}\, \mathrm{x}_2 - \mathrm{K}_2)$ and demonstrates the renormalization operator. Here, two diadic sub-bands $\left[2^{2\mathrm{b}}\ , 2^{2\mathrm{b}+1}\ \right]$and $\left[2^{2\mathrm{b}+1}\ , 2^{2\mathrm{b}+2}\ \right]$are integrated before implementing ridgelet transform. Finally, the ridgelet transform is performed after the renormalization step and it is described by equation(3).

$$\propto_{\mu} = \langle \mathrm{h_Q}\ , \mathrm{p}\lambda \rangle \qquad (3)$$

The de-noising results after applying Curvelet transform are represented in **Figure 4**.

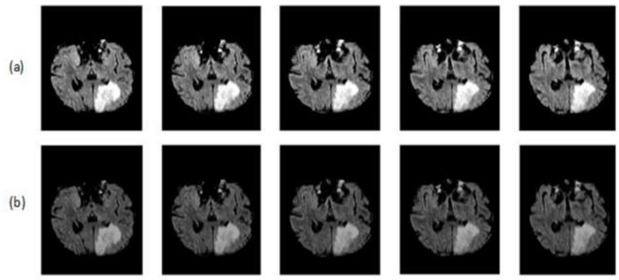

Figure 4: Image de-noising by implementing Curvelet transform using MRI images of brain from BRATS 2013 dataset. The upper row(a) represents original images while below row(b) explains enhanced images after Curvelet transform.

3.2. ACO and thresholding based tumor extraction

In medical field, image segmentation is an essential and vital step due to its significance for the process of infection detection. The challenges of tumor such as irregular shape and change of texture are major limitations of this domain. These limitations affect overall accuracy and complexity of segmentation process. There are many methods used to overcome these limitations such as expectation maximization (EM), Otsu thresholding, Watershed and few more. In this research, a hybrid approach named asACO and thresholding method for tumor segmentation are implemented. ACO(X. Wang, Ouyang, Zhu, Yu, & Li, 2019) is employed for edge detection and it is used with thresholding for the extraction of tumor region from a brain image. The input image is regarded a graph which basically is two dimensional and its nodes are pixels of image. Ants travel from one pixel to another one on the graph for the sake of making a pheromone matrix whose every single entry is responsible for representing the edge information around every solo pixel site in an image. The relocation of ants is organized with the help of heuristic information. These ants alter their site in the image in accordance with the rules of transition and after that leave a pheromone particular quantity on those nodes that were visited by them. As much as the ants follow a track, the same amount or size of pheromone is observed. This eventually makes this trail more attractive for many other ants. Finally, the outcomes of detection of edges can be acquired by doing an analysis of pheromone dispersal in the image. This technique implementation details are given as under:

I. Starting Ant Distribution

Mostly, the quantity of ants is calculated mathematically by using equation (4).

$$N = \sqrt{A \times B} \tag{4}$$

Where, A = length of an input image, B = width of an input image and N is for the random placement of ants with an arrangement that at maximum only one ant can be on each pixel.

II. Decision based on probability

An ant n travels with a probability p_{ij} from pixel (i,j) to pixel (k, l). The value of probability is calculated by equation (5).

$$p_{ij} = \frac{(\sigma_{ij})^{\alpha}(\mu_{ij})^{\beta} w_{ij}(\Delta)}{\sum_{j \in Q}(\sigma_{ij})^{\alpha}(\mu_{ij})^{\beta} w_{ij}(\Delta)}, \text{when } i, j \in \Omega \tag{5}$$

Where, all the values of pixel locations which are 8-neighbourhood of recent pixel (i,j) are shown by i, j∈ Ω. σ_{ij} symbolizes the amount of pheromone. μ_{ij} denotes the visibility whose value is described by using the function given in equation (6).

$$\mu_{ij} = G_{ij} \tag{6}$$

In equation of probability, the amount of variations in direction at each stage is calculated by Δplus it can use discrete or distinct value. This is given in equation (7).

$$\Delta = 0, \frac{\pi}{4}, \frac{\pi}{2}, \frac{3\pi}{4}, \pi. \tag{7}$$

Where, w(Δ) symbolizesweighting function plus this function makes sure that the probability of very sudden plus sharp turns is less in comparison to the turns with smaller angles, hence every ant of colony retains a probabilistic bias in onward direction.

III. Rules of Transition

The variable n represent an ant placed at pixel location (i, j) will travel to pixel location (k, l) with respect to equation (8)

$$s = \begin{Bmatrix} \arg\left\{\max_{j \in \Omega}\left[(\sigma_{ij})^{\alpha}(\mu_{ij})^{\beta} w_{ij}(\Delta)\right]\right\} \\ S \end{Bmatrix}, \text{when } q \le q_0$$

(8)

If $q > q_0$, ants have the ability to choose next pixel for visiting as demonstrated by the probability distribution shown in part II.

IV. Updating pheromone

The matrix of pheromone is required to be changed two times while ACO process is still going on. First of all, once an ant gets transferred from the recent pixel (i, j) to the afterward pixel (k, l), the pheromone trajectory of its path is altered as given under in equation (9 and 10).

$$\sigma_{ij} = (1 - \gamma).\sigma_{ij} + \gamma.\Delta\sigma_{ij} \tag{9}$$

$$\Delta\sigma_{ij} = \mu_{ij} \tag{10}$$

Where, $\gamma (0 < \gamma < 1)$ shows the ratio of evaporation of pheromone.

The next change signifies global change on all the routes despite or not a route has been traversed. The pheromone gets new value after each round and the matrix of pheromone is updated accordingly as follows by equation (11).

$$\sigma_{ij} = (1 - \theta).\sigma_{ij} + \theta.\sigma_0 \tag{11}$$

Where, $\theta (0 < \theta < 1)$ denotes the ratio of pheromone evaporation and σ_0 illustrates the pheromone starting value.

V. Procedure of final decision

A pre-determined number of rounds are used to set the end of algorithm; each of such cycles is comprised of fixed stages. At last, a binary decision is taken at every pixel site in order to decide if it was present on the outside border or not. This is done by implementing a threshold value T on the concluding resultant pheromone matrix.

Finally, irrelevant regions are removed with the help of thresholding and its results are presented in Figures 5 and 6.

3.3. Feature Extraction

Feature extraction is a vital stage in ML to classify objects into their relevant category(Khan, Akram, Sharif, Javed, et al., 2018; Khan et al., 2017; Sharif et al., 2017; Sharif, Khan, Faisal, Yasmin, & Fernandes, 2018). Several categories of features are extracted in literature plus each feature has its own properties(Khan, Akram, Sharif, Awais, et al., 2018; Rashid et al., 2018; Sharif, Khan, Iqbal, et al., 2018). In this paper, exact location of tumor in brain MRI scans is determined after the extraction of shape as well as texture features.

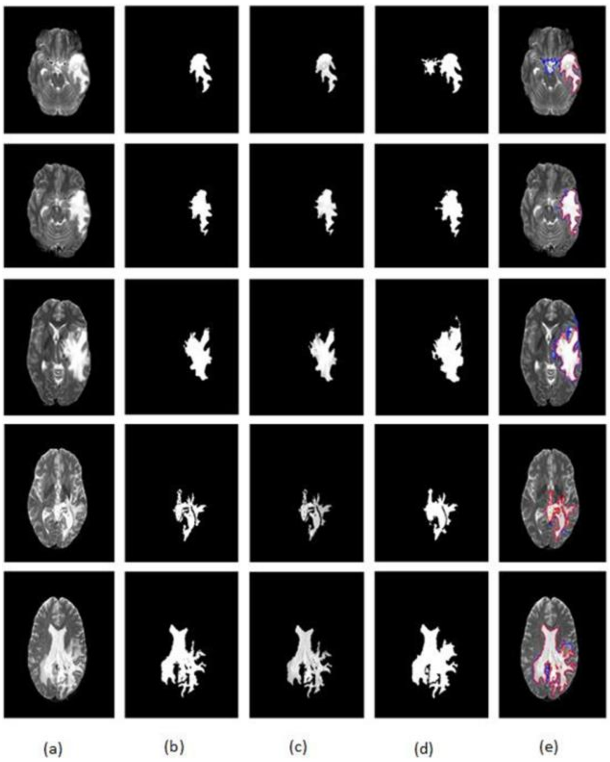

Figure 5: Brain tumor segmentation results based on hybrid technique of ACO+Thresholding using private dataset.(a)Original image (b)Segmented image using ACO+Thresholding (c)Mapped image (d)Ground truth image (e)Mapping of segmented image with ground truth image

The performance accuracy of any method is dependent on the extraction process of most robust and active set of features. LBP and SFTA features exist in the set of local features and extracted to get information about texture whereas HOG descriptors are lies in the set of global features because of shap einformation. Furthermore, the explanation of all extracted feature is presented below.

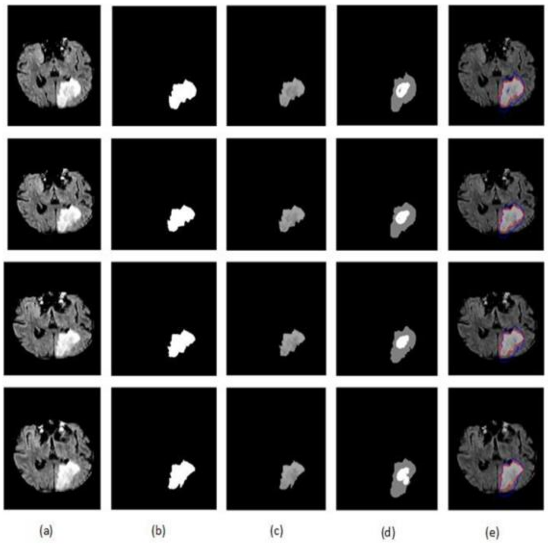

Figure 6: Results of brain tumor segmentation using hybrid system of ACO+Thresholding using BRATS 2013 dataset.(a)Actual image (b)Image with segmentation using ACO+Thresholding (c)Plotted image (d)image of Ground truth (e)Plotting of segmented image with ground truth image

3.3.1. LBP

Local binary pattern(LBP) features also known as texture patterns are utilized in many ML applications because of low computational time, simplicity and robustness (Rajesh & Malar, 2017).Mathematically, LBP features are computed as follows in equation (12).

$$\mathrm{LBP}_{\mathrm{T,r}} = \sum_{\mathrm{k=0}}^{\mathrm{T-1}} \mathrm{s}(\mathrm{h_k} - \mathrm{h_c})2^{\mathrm{k}}, \tag{12}$$

Where, S(x) = {1, if x>= 0 |0, if x<0}(Yang, Yang, Zhang, & Lu, 2003). The variable Tsymbolizes the number of pixels present in matrix, rsymbolizesthe radius of corresponding matrix, $\mathrm{h_k}$is current pixel value and $\mathrm{h_c}$ is central pixel value. This formulation provides a binary bit string which is further converted to decimal string and then finally converted into histogram. The resultant feature vector is obtained after converted into histograms of dimension $\mathrm{N} \times 59$.

3.3.2. Histogram of oriented gradient

In the second phase, the extraction of features named as Histogram of oriented gradient (HOG)is performed on segmented tumor images. As (Y. Wang, Zhu, & Wu, 2018) identification ofanobject with the help of its shape is accomplished using HOG features, therefore the detection accuracy of shape and appearance of object depends upon dispersion of local intensity gradient and edge detection. There are four steps involved in HOG feature extraction which includes gradient calculation, separation of blocks and cells, normalization of blocks and vector calculation. In the gradient calculation step, horizontal and vertical gradients are computed by using mask$[-1\ 0\ 1]^{T}$and $[-1\ 0\ 1]$ respectively. Mathematically, the mask is defined as follows by equations (13) and (14).

$$K_x(x,y) = L(x+1,y) - L(x-1,y) \quad (13)$$

$$K_y(x,y) = L(x,y+1) - L(x,y-1) \quad (14)$$

When, $L(x,y)$is the representation of pixel values, $K_x(x,y)$ denotes the horizontal axis direction and $K_y(x,y)$ is vertical direction respectively. Then in the second step, the orientation and magnitude are computed by following mathematical formulation given in equations (15) and (16).

$$K(x,y) = \sqrt{K_x(x,y)^2 + K_y(x,y)^2} \quad (15)$$

$$b(x,y) = \tan^{-1}\left(\frac{K_y(x,y)}{K_x(x,y)}\right) \quad (16)$$

Where, $K(x,y)$ describes the magnitude and $b(x,y)$is gradient direction.Afterwards, the input image is distributed into sections and each section is converted in to cells of size 8×8. Each 8×8 cell contains 192 values. Moreover, histogram with 9 bin values is used for the representation of these values and later on these value store into an array. The next step is about normalization block cell of size 16×16 using the mathematical formulation as follows in equations (17) to (19).

$$V = [a_1, a_2, a_3, \ldots\ldots\ldots a_q] \quad (17)$$

$$VL = \sqrt{a_1^{\,2} + a_2^{\,2} + a_3^{\,2} + \cdots \ldots\ldots a_q^{\,2}} \quad (18)$$

$$VN = \left[\frac{a_1}{VL}, \frac{a_2}{VL}, \frac{a_3}{VL}, \ldots\ldots\ldots\ldots\ldots \frac{a_q}{VL}\right] \quad (19)$$

Where,V denotes the extracted vector, VLrepresents the length of vector which is equal to norm and VNshows the normalized vector respectively.Finally, a resultant vector of dimension N× 3780 is obtained.

3.3.3. Fractal Texture Analysis based on Segmentation (SFTA)

The complexity and features based on texture in an image is demonstrated by SFTA (Costa, Humpire-Mamani, & Traina, 2012; Zhelezniakov et al., 2015) using fractal dimension analysis. SFTA is very useful for the classification of texture. The SFTA features are computed in two steps, firstly a bunch of binary images is attained through division of segmented image. Secondly, the computation of fractal dimension is performed on sections of the binary image. The posterior probabilities, as given in equation (20), are calculated after giving ‘a’ to SFTA feature vector for each class C_n showing an earlier identified individual in a database.

$$p(C_n|a) = \frac{p(C_n)p(a|C_n)}{p(a)} \quad (20)$$

Where, class prior $p(C_n)$ are computed by assuming classes as equi-probable. The ranking of classes depends upon posterior probabilities. Finally, a group of similar matches can be presented for decision making.

3.4. Feature Reduction and Fusion

In this step, a new technique named PCA reduced skewness (PCArS) is proposed for feature reduction. The proposed PCArS approach consists of two core steps- PCA based principle score (PS) calculation and skewness calculated from PS to reduce irrelevant features from each feature set. The resultants FVs are fused with respect to the simple serial based concatenation process after reducing irrelevant features. Mathematically, the reduction and fusion process is defined as follows.

Let F_1, F_2 and F_3 are three extracted feature vectors LBP, HOG and SFTA whereas the dimension of each vector is $N \times 59$, $N \times 3780$ and $N \times 21$ correspondingly. Let F_{s1}, F_{s2} and F_{s3} denote the principle score values (PSV) of each FV which is mathematically formulated by equation (21).

$$\widetilde{F_k(\imath\jmath)} = \overline{F}_\imath + z_{kj}M_{ki} \quad (21)$$

Where, $\widetilde{F_k(\imath\jmath)}$ denote the prediction of ith observation, i and j are rows and columns pixels, and M is anp × p principle matrix. The variable $\overline{F}_\imath$ is centroid or mean point of extracted vector. The PSV are computed for all three vectors F_1, F_2, and F_3. After that, by utilizing PSV $\widetilde{F_k(\imath\jmath)}$, we compute the skewness vector by using ith pixels as:

$$S(i)^h = \frac{\sum_{i=1}^{N}(\mathbf{F_i} - \overline{\mathbf{F}})^3|\mathbf{N}}{(\sigma)^3} \quad (22)$$

Where,$\overline{\mathbf{F}}$denotes the mean value, $\boldsymbol{\sigma}$ is standard deviation and $\mathbf{N}$ are total number of data points. The variable $\mathbf{h} \in (1,2,3)$ of LBP, HOG and SFTA skewness vector. After that, only positive skewness values are considered for reduced FVs and serial based fusion is performed (Yang et al., 2003). Finally, top 70% features are selected from fused vector and fed to multi-SVM of kernel function (RBF)where number of splits is automatic.

4. RESULTS

In this part, experimental results of proposed segmentation and classification approach are described in both qualitative and quantitative form. The new proposed system results are tested using two datasets- Private collected images and BRATS 2013. Privately collected dataset comprises a total of 40 healthy as well as 40unhealthy MRI scans while on the other hand BRATS 2013 dataset includes a total of 30 subjects (20 HG and 10 LG MRI scans). These scans include malignant, benign and healthy images. Two different types of results are computed for the analysis of proposed framework- segmentation results on selective Private and BRATS 2013 dataset and classification. The proposed classification performance is measured and compared with recently implemented classification algorithms such as ensemble trees and decision trees. The analysis of these classifiers is done through well-known performance metrics including sensitivity, precision, accuracy and FNR.

4.1. Accuracy measure of segmentation

The accuracy of segmentation results is analyzed in this section on both Private collected scans and few BRATS 2013 dataset respectively. The dice (D) parameter is computed for validation of segmentation performance. The results are shown in Tables 1 and 2 for given two datasets.

Some sample results alongside images of ground truth are presented in Table 1to compute the average dice value of 90.81% which is significantly good.100% accuracy is not possible in this case due to several factors such as change of tumor place, size and orientation. In Table 2, segmentation results of BRATS 2013 dataset are presented and achieved average segmentation dice is 95.29% and FNR is 4.3%. The results are obtained through provided ground truth images. In Tables 1 and 2, each row consists of following sequence- original scan, edges extraction, proposed segmented tumor, corresponding ground truth image, boundary extraction and dice value. The average segmentation results demonstrate that the ACO along thresholding approach outperforms on both given datasets with respect to the dice value.

Table 1: Segmentation results of ACO along thresholding on BRATS 2013 dataset

Actual Image	Edges Extraction	Segmented Image	Ground truth	Boundary image	Dice value
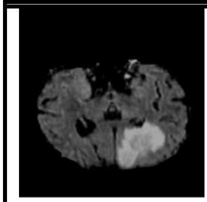	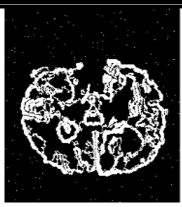	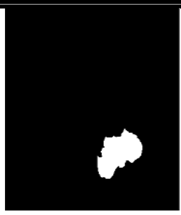	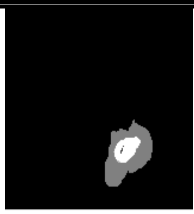	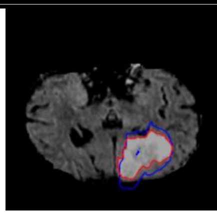	0.9034
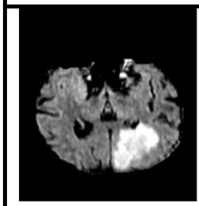	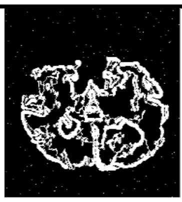	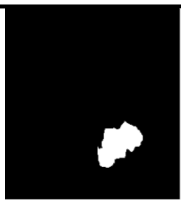	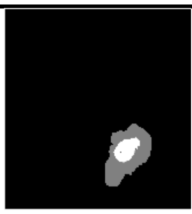	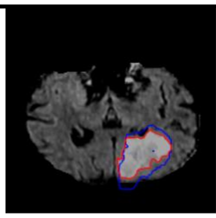	0.9006
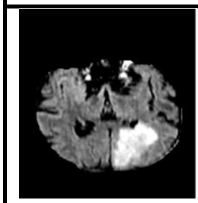	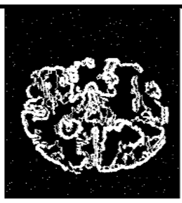	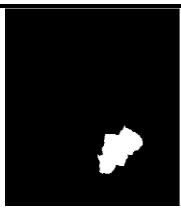	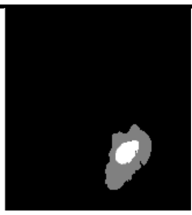	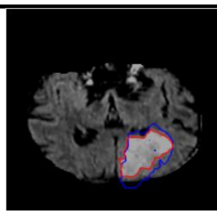	0.8896
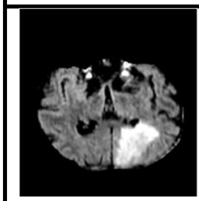	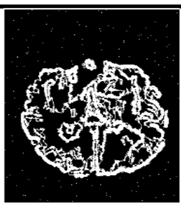		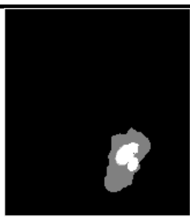	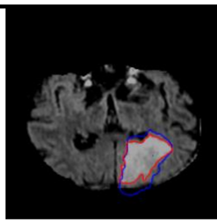	0.8994
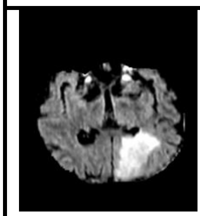	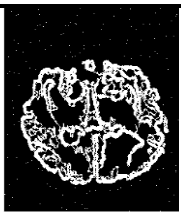			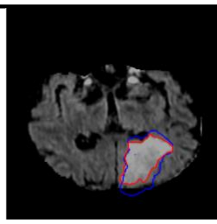	0.9052
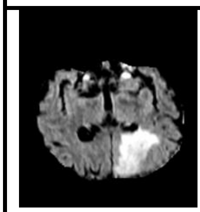	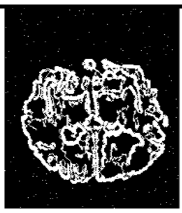	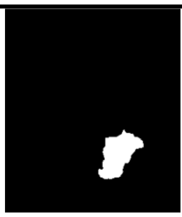	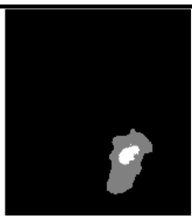	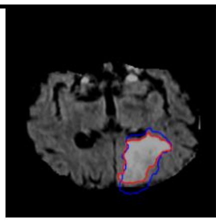	0.9109

Table 2: Segmentation results of ACO along thresholding on Private collected MRI scans

4.2. Accuracy measure of classification

In this part, results of proposed classification approach are tested by using two datasets- BRATS 2013 as well as Privately collected dataset. The accuracy of classification is measured through five performance metrics as discussed above. A 60:40 approach is selected which explains that the training is performed on 60% of MRI scans from both datasets and testing is performed on remaining 40% scans. All results are computed through K-fold cross validation where K=10.

There are three steps involves for computation of classification results using BRATS 2013 dataset- Fusion of reduced features after PCArS approach, presented in Table 3. The maximum achieved accuracy of this step is 90.3% which is verified by Table 4. The other best achieved performance measures which are known as sensitivity, precision, AUC and FNR are 84.30%, 88.67%, 0.940, and 9.7%, respectively.

In the second step, the results of classification are computed on top 70% features and achieved best accuracy of 92% on MSVM, shown in Table 5. The other calculated parameters as sensitivity, precision, AUC and FNR are 91.33%, 91.67%, 0.903, and 8%, respectively. These results are also verified by Table 6.

The top 50% features are selected to perform classification, in the third step. The achieved maximum accuracy is 94.7% and results are demonstrated in Table 7 and verified by Table 8. The overall results of classification by using BRATS 2013 dataset demonstrates that the selection of 50% priority features gives better accuracy as compared to 70% top priority selected features and fusion of reduced feature vectors. Moreover, it is also clearly shown that MSVM outperforms as compared to ensemble and decision trees classification techniques.

In addition, the classification results of Private collected MRI scans are presented in Table 9. The maximum achieved accuracy of MSVM on 50% reduced features is 94.6% which is verified by Table 10. The other SVM Kernel functions also give good accuracy of 94.4% which shows the consistency of overall results on Private dataset.

Table 3: Results of PCArS reduced features fusion by using data set of BRATS 2013

Met	Performance Measures				
	Sen (%)	Pre (%)	AUC	Acc (%)	FNR (%)
Linear SVM	68.00	91.00	0.940	86.2	13.8
Quadratic SVM	80.00	84.00	0.936	89.4	10.6
Cubic SVM	75.67	82.00	0.917	88.4	11.6
Fine KNN	80.00	82.67	0.860	89.4	10.6
Cubic KNN	35.00	85.30	0.760	62.3	37.7
Cosine KNN	76.33	88.30	0.976	88.3	11.7
Fine Tree	69.33	71.00	0.830	77.4	22.6
Boosted Trees	70.67	79.00	0.927	80.7	19.3
Bagged Trees	49.00	58.33	0.810	70.9	29.1
MSVM	**89.67**	**88.67**	0.940	**90.3**	**9.7**

Table 4: Results of Confusion matrix of PCArS reduced features fusion by using data set of BRATS 2013

Category	Category		
	Benign	Melanoma	Healthy
Benign	**92%**	4%	4%
Melanoma	9%	**84%**	3%
Healthy	6%	1%	**93%**

Table 5: Results of

Proposed 70% priority features selection by using data set of BRATS 2013

Method	**Performance Measures**				
	Sensitivity (%)	Precision (%)	AUC	Accuracy (%)	FNR (%)
Linear SVM	77.00	81.00	0.950	84.4	15.6
Q SVM	82.00	83.00	0.963	88.4	11.6
Cubic SVM	83.33	84.00	0.963	89.8	10.2
Fine KNN	85.13	86.67	0.903	92.0	8.0
Cubic KNN	73.00	84.00	0.953	84.1	15.9
Cosine KNN	81.67	89.00	0.983	89.1	10.9
Fine Tree	67.00	69.67	0.817	76.8	23.2
BT	67.33	73.33	0.900	77.1	22.9
Bagged Trees	80.00	82.00	0.927	86.8	13.2
MSVM	**91.33**	**91.67**	**0.903**	**92.0**	**8.0**

Table 6: Results of Confusion matrix of 70% priority features selection by using BRATS 2013

Category	**Category**		
	Benign	Melanoma	Healthy
Benign	**94%**	4%	2%
Melanoma	30%	**86%**	2%
Healthy	5%	1%	**94%**

Table 7: Results of Proposed classification on 50% top priority selected features by using BRATS 2013

Method	**Performance Measures**				
	Sensitivity (%)	Precision (%)	AUC	Accuracy (%)	FNR (%)
Linear SVM	93.33	93.67	0.993	93.6	6.4
QSVM	92.67	93.00	0.983	92.8	7.2
Cubic SVM	92.33	92.67	0.983	92.4	7.6
Fine KNN	94.00	94.37	0.960	93.7	6.3
Cubic KNN	87.00	88.00	0.963	87.1	12.9
Cosine KNN	86.33	89.67	0.970	86.4	13.6
Fine Tree	82.00	82.00	0.890	82.2	17.8
Bagged Trees	91.33	91.67	0.977	91.3	8.7
SDA	94.33	94.33	0.993	94.3	5.7
MSVM	**94.33**	**94.67**	0.957	**94.7**	**5.3**

Table 8: Confusion matrix of top 50% selected features

Category	**Category**		
	Benign	Melanoma	Healthy
Benign	94%	6%	
Melanoma	5%	94%	1%
Healthy	3%	1%	95%

Table 9: Proposed classification results on Private collected MRI scans

Classifier	**Performance Measures**				
	Sensitivity (%)	Precision (%)	AUC	Accuracy (%)	FNR (%)
Linear SVM	94.5	95.0	0.89	94.4	5.6
QSVM	89.0	89.0	0.89	88.9	11.1
Cubic SVM	89.0	89.0	0.83	88.9	11.1
CGSVM	94.5	95.0	0.89	94.4	5.6
Cubic KNN	94.3	95.0	0.93	94.4	5.6
Cosine KNN	94.3	95.0	0.94	94.4	5.6
MKNN	94.3	95.0	0.94	94.4	5.6
Bagged Trees	89.0	89.0	0.94	88.9	11.1
EBT	89.0	91.0	1.00	88.9	11.1
M-SVM	**94.5**	**95.2**	**0.98**	**94.6**	**5.4**

Table 10: Confusion matrix of Private collected dataset

Category	**Category**	
	Healthy	Unhealthy
Healthy	**90%**	11%
Unhealthy		**100%**

4.3. Discussion and Comparison

The detail discussion and comparison of proposed method is described in this section. There are five primary steps involved in this research as demonstrated in Figure 3. The first step is used for enhancement of an image, curvelet based transformation is employed and visual outputs are represented in Figure 4. As a second step, ACO plus thresholding approach is proposed for tumor segmentation whose effects are shown in Figures 5 and 6. In the third step, multi properties features are extracted which are reduced in the fourth step by PCArS approach. In the final step, top 50% priority features are picked and are transferred to MSVM for the sake of classification. In the results section, initially the segmentation results are presented in Tables 1 and2 for BRATS 2013 and Private collected datasets respectively. The overall achieved dice is higher than 90%. Finally, the classification results are presented in Tables 3-10 for both datasets and maximum achieved accuracy of 94% and 94.6% respectively. The accuracy of classification using BRATS 2013 dataset is computed in three steps- fusion of reduce feature vectors, selection of top 70% priority features and 50% top priority features. The overall results are demonstrating clearly that the system proposed gives best performance for selecting top 50% features.

Further,Table11 provides a comparison of proposed method and already implemented techniques in terms of accuracy measure.Reza.et al. proposed an approach based on texture features for classifying tumor, with accuracy 86.70% which was tested upon BRATS 2013 dataset and this approach. While this research concludes that segmentation is improved with the help of hybrid technique of ACO and thresholding. The proposed hybrid segmentation method is implemented using BRATS 2013 dataset and Private dataset providing an accuracy of 91.09% and 99.77% respectively. Moreover, best classification results are attained by using skewness controlled PCA for features selection with an accuracy of 94.7% and 94.4% for BRATS 2013 and Private datasets correspondingly.

Table 11: Comparison with existing techniques using BRATS 2013 dataset

Method	Year	Dataset	Accuracy
(Cordier, Menze, Delingette, & Ayache, 2013)	2013	BRATS 2013	84.00%
(Reza, Mays, & Iftekharuddin, 2015)	2015	BRATS 2013	86.70%
(Abbasi & Tajeripour, 2017)	2017	BRATS 2013	93.00%
Proposed	**2019**	**BRATS 2013**	**94.70%**

5. Conclusion

Lately, many computer vision techniques are developed by several researchers to detect and classify brain tumor from MRI scans. The automated process helps doctors in identifying brain tumor. In this particular paper, a unified framework has been proposed to segment and classify brain tumor that is comprisedof five primary steps. Curvelet transform is applied for tumor visibility enhancement which is later segmented through ACO along with thresholding method. Mixtures of texture and shape features are extracted and reduced through PCArS approach and serially fused all of them. Later, results are computed on all fused features, top 70% priority features and 50% features. The classification accuracy of top 50% features is shown best as compared to others. From results, it is concluded that better segmentation of tumor provides good features which later on provide best accuracy. Moreover, it is also clear that the reduction of 50% features gives better accuracy whereas on 70% features, the results are consistent for all datasets.

In future, the accuracy and efficiency of system can be improved by implementing deep learning. Deep learning is very popular among researchers these days and it can help to make system automated with great accuracy and efficiency. The proposed unified framework has some limitations such as selection of only top 70% and 50% features and over segmentation which will be overcome in future.

Acknowledgement

Prince Sultan University Riyadh KSA, Grant/Award Number: 11-02-2019

6. REFERENCES

Abbasi, S., & Tajeripour, F. (2017). Detection of brain tumor in 3D MRI images using local binary patterns and histogram orientation gradient. *Neurocomputing, 219*, 526-535.

Akram, T., Khan, M. A., Sharif, M., & Yasmin, M. (2018). Skin lesion segmentation and recognition using multichannel saliency estimation and M-SVM on selected serially fused features. *Journal of Ambient Intelligence and Humanized Computing*, 1-20.

Anitha, R., & Siva Sundhara Raja, D. (2018). Development of computer-aided approach for brain tumor detection using random forest classifier. *International Journal of Imaging Systems and Technology, 28*(1), 48-53.

Ariyo, O., Zhi-guang, Q., & Tian, L. (2017). Brain MR Segmentation using a Fusion of K-Means and Spatial Fuzzy C-Means. *DEStech Transactions on Computer Science and Engineering*(csae).

Bahadure, N. B., Ray, A. K., & Thethi, H. P. (2018). Comparative Approach of MRI-Based Brain Tumor Segmentation and Classification Using Genetic Algorithm. *Journal of digital imaging*, 1-13.

Buerki, R. A., Chheda, Z. S., & Okada, H. (2018). Immunotherapy of Primary Brain Tumors: Facts and Hopes. *Clinical Cancer Research, 24*(21), 5198-5205.

Cordier, N., Menze, B., Delingette, H., & Ayache, N. (2013). *Patch-based segmentation of brain tissues.* Paper presented at the MICCAI challenge on multimodal brain tumor segmentation.

Costa, A. F., Humpire-Mamani, G., & Traina, A. J. M. (2012). *An efficient algorithm for fractal analysis of textures.* Paper presented at the Graphics, Patterns and Images (SIBGRAPI), 2012 25th SIBGRAPI Conference on.

Damodharan, S., & Raghavan, D. (2015). Combining Tissue Segmentation and Neural Network for Brain Tumor Detection. *International Arab Journal of Information Technology (IAJIT), 12*(1).

Drozdzal, M., Chartrand, G., Vorontsov, E., Shakeri, M., Di Jorio, L., Tang, A., . . . Kadoury, S. (2018). Learning normalized inputs for iterative estimation in medical image segmentation. *Medical image analysis, 44*, 1-13.

Kalavathi, P., & Prasath, V. S. (2016). Methods on skull stripping of MRI head scan images—A review. *Journal of digital imaging, 29*(3), 365-379.

Khan, M. A., Akram, T., Sharif, M., Awais, M., Javed, K., Ali, H., & Saba, T. (2018). CCDF: Automatic system for segmentation and recognition of fruit crops diseases based on correlation coefficient and deep CNN features. *Computers and electronics in agriculture, 155*, 220-236.

Khan, M. A., Akram, T., Sharif, M., Javed, M. Y., Muhammad, N., & Yasmin, M. (2018). An implementation of optimized framework for action classification using multilayers neural network on selected fused features. *Pattern Analysis and Applications*, 1-21.

Khan, M. A., Sharif, M., Javed, M. Y., Akram, T., Yasmin, M., & Saba, T. (2017). License number plate recognition system using entropy-based features selection approach with SVM. *IET Image Processing, 12*(2), 200-209.

LIAQAT, A., KHAN, M. A., SHAH, J. H., SHARIF, M., YASMIN, M., & FERNANDES, S. L. (2018). AUTOMATED ULCER AND BLEEDING CLASSIFICATION FROM WCE IMAGES USING MULTIPLE FEATURES FUSION AND SELECTION. *Journal of Mechanics in Medicine and Biology*, 1850038.

Liu, J., Li, M., Wang, J., Wu, F., Liu, T., & Pan, Y. (2014). A survey of MRI-based brain tumor segmentation methods. *Tsinghua Science and Technology, 19*(6), 578-595.

Mohsen, H., El-Dahshan, E.-S. A., El-Horbaty, E.-S. M., & Salem, A.-B. M. (2018). Classification using deep learning neural networks for brain tumors. *Future Computing and Informatics Journal, 3*(1), 68-71.

Nasir, M., Attique Khan, M., Sharif, M., Lali, I. U., Saba, T., & Iqbal, T. (2018). An improved strategy for skin lesion detection and classification using uniform segmentation and feature selection based approach. *Microscopy research and technique*.

Pereira, S., Pinto, A., Alves, V., & Silva, C. A. (2016). Brain tumor segmentation using convolutional neural networks in MRI images. *IEEE transactions on medical imaging, 35*(5), 1240-1251.

Rajesh, T., & Malar, R. (2017). Robust Classification of Brain Tumor in MRI Images using Salient Structure Descriptor and RBF Kernel-SVM. *Asian Journal of Research in Social Sciences and Humanities, 7*(2), 58-71.

Rashid, M., Khan, M. A., Sharif, M., Raza, M., Sarfraz, M. M., & Afza, F. (2018). Object detection and classification: a joint selection and fusion strategy of deep convolutional neural network and SIFT point features. *Multimedia Tools and Applications*, 1-27.

Reza, S. M., Mays, R., & Iftekharuddin, K. M. (2015). *Multi-fractal detrended texture feature for brain tumor classification.* Paper presented at the Medical Imaging 2015: Computer-Aided Diagnosis.

Roberts, T., Hyare, H., Hipwell, B., Ianus, A., Breen-norris, J., Panagiotaki, E., . . . Brandner, S. (2018). Quantification of tumour microstructure in low and high-grade brain tumours using VERDICT MRI: an initial feasibility study. *Neuro-oncology, 20*(suppl_1), i16-i16.

Routray, S., Ray, A. K., & Mishra, C. (2018). Image denoising by preserving geometric components based on weighted bilateral filter and curvelet transform. *Optik, 159*, 333-343.

Sharif, M., Khan, M. A., Akram, T., Javed, M. Y., Saba, T., & Rehman, A. (2017). A framework of human detection and action recognition based on uniform segmentation and combination of Euclidean distance and joint entropy-based features selection. *EURASIP Journal on Image and Video Processing, 2017*(1), 89.

Sharif, M., Khan, M. A., Faisal, M., Yasmin, M., & Fernandes, S. L. (2018). A framework for offline signature verification system: Best features selection approach. *Pattern Recognition Letters*.

Sharif, M., Khan, M. A., Iqbal, Z., Azam, M. F., Lali, M. I. U., & Javed, M. Y. (2018). Detection and classification of citrus diseases in agriculture based on optimized weighted segmentation and feature selection. *Computers and Electronics in Agriculture, 150*, 220-234.

Sharif, M., Tanvir, U., Munir, E. U., Khan, M. A., & Yasmin, M. (2018). Brain tumor segmentation and classification by improved binomial thresholding and multi-features selection. *Journal of Ambient Intelligence and Humanized Computing*, 1-20.

Sharma, M., Purohit, G., & Mukherjee, S. (2018). Information retrieves from brain MRI images for tumor detection using hybrid technique K-means and artificial neural network (KMANN) *Networking communication and data knowledge engineering* (pp. 145-157): Springer.

Starck, J.-L., Candès, E. J., & Donoho, D. L. (2002). The curvelet transform for image denoising. *IEEE Transactions on image processing, 11*(6), 670-684.

Wang, X., Ouyang, J., Zhu, Y., Yu, H., & Li, H. (2019). A Novel Medical Image Edge Detection Method Based on Reinforcement Learning and Ant Colony Optimization. *Journal of Medical Imaging and Health Informatics, 9*(1), 175-182.

Wang, Y., Zhu, X., & Wu, B. (2018). Automatic detection of individual oil palm trees from UAV images using HOG features and an SVM classifier. *International Journal of Remote Sensing*, 1-15.

Yang, J., Yang, J.-y., Zhang, D., & Lu, J.-f. (2003). Feature fusion: parallel strategy vs. serial strategy. *Pattern recognition, 36*(6), 1369-1381.

Zhang, W., Li, R., Deng, H., Wang, L., Lin, W., Ji, S., & Shen, D. (2015). Deep convolutional neural networks for multi-modality isointense infant brain image segmentation. *NeuroImage, 108*, 214-224.

Zhelezniakov, A., Eerola, T., Koivuniemi, M., Auttila, M., Levänen, R., Niemi, M., . . . Kälviäinen, H. (2015). *Segmentation of saimaa ringed seals for identification purposes.* Paper presented at the International Symposium on Visual Computing.